the FEBS Journal

Substrate specificity and the effect of calcium on *Trypanosoma brucei* metacaspase 2

Maurício F. M. Machado[1], Marcelo F. Marcondes[1], Maria A. Juliano[1], Karen McLuskey[2], Jeremy C. Mottram[2], Catherine X. Moss[2], Luiz Juliano[1] and Vitor Oliveira[1]

1 Department of Biophysics, Escola Paulista de Medicina, Universidade Federal de São Paulo, Brazil
2 Wellcome Trust Centre for Molecular Parasitology, Institute of Infection Immunity and Inflammation, College of Medical Veterinary and Life Sciences, University of Glasgow, UK

Keywords
calcium binding; kinetic parameters; metacaspase; structural modification; substrate specificity

Correspondence
V. Oliveira, Departamento de Biofísica, Laboratório de Enzimologia, Universidade Federal de São Paulo, Rua Pedro de Toledo, 669 – 7° andar, São Paulo 04039-032, SP, Brazil
Fax: +55 11 55759617
Tel: +55 11 55764450 ext 1966
E-mail: vitor.oliveira@unifesp.br

(Received 30 November 2012, revised 19 February 2013, accepted 11 March 2013)

doi:10.1111/febs.12248

Metacaspases are cysteine peptidases found only in yeast, plants and lower eukaryotes, including the protozoa. To investigate the extended substrate specificity and effects of Ca^{2+} on the activation of these enzymes, detailed kinetic, biochemical and structural analyses were carried out on metacaspase 2 from *Trypanosoma brucei* (TbMCA2). These results reveal that TbMCA2 has an unambiguous preference for basic amino acids at the P_1 position of peptide substrates and that this is most probably a result of hydrogen bonding from the P_1 residue to Asp95 and Asp211 in TbMCA2. In addition, TbMCA2 also has a preference for charged residues at the P_2 and P_3 positions and for small residues at the prime side of a peptide substrate. Studies into the effects of Ca^{2+} on the enzyme revealed the presence of two Ca^{2+} binding sites and a reversible structural modification of the enzyme upon Ca^{2+} binding. In addition, the concentration of Ca^{2+} used for activation of TbMCA2 was found to produce a differential effect on the activity of TbMCA2, but only when a series of peptides that differed in P_2 were examined, suggesting that Ca^{2+} activation of TbMCA2 has a structural effect on the enzyme in the vicinity of the S_2 binding pocket. Collectively, these data give new insights into the substrate specificity and Ca^{2+} activation of TbMCA2. This provides important functional details and leads to a better understanding of metacaspases, which are known to play an important role in trypanosomes and make attractive drug targets due to their absence in humans.

Introduction

Metacaspases are cysteine peptidases that are distantly related to the mammalian caspases but found only in plants, fungi and protozoa [1]. Together with the caspases and paracaspases [1], they are endopeptidases which have been grouped into structural family C14 in clan CD of the MEROPS peptidase database [2]. In *Trypanosoma brucei*, five metacaspase genes (*TbMCA1–5*) have been reported with three, *TbMCA2*, *TbMCA3* and *TbMCA5*, predicted to code for active peptidases based on the conservation of an intact cysteine-histidine catalytic dyad [3,4]. Interestingly, in TbMCA1 and TbMCA4 the catalytic cysteine is replaced by a serine, indicating that the coded proteins would not exhibit cysteine peptidase activity [3,5]. Whilst plant metacaspases have been shown to be involved in cell death pathways, trypanosomes appear to lack regulated cell death [6] and in these organisms metacaspases have evolved alternative functions [5,7].

Abbreviations
Abz, *ortho*-aminobenzoic acid; EDDnp, *N*-(2,4-dinitrophenyl)-ethylenediamine; FRET, fluorescence resonance energy transfer; TbMCA2, *Trypanosoma brucei* metacaspase 2.

Despite being related to the caspases, metacaspases have been shown to be both structurally and functionally distinct. Metacaspases are known to cleave their substrates after Arg and Lys residues in the P_1 position [8], as demonstrated for metacaspases from *Trypanosoma brucei* [9], *Trypanosoma cruzi* [10], *Leishmania major* [11], plants [12–14] and yeast [13], while the caspases cleave their substrates after Asp [15]. Other functional differences between the two families of enzymes are that, unlike the caspases, metacaspases do not necessarily require processing or dimerization for activity and they are activated by calcium [9,12–14,16]. In addition, the recent crystallographic structures of TbMCA2 and the *Saccharomyces cerevisiae* metacaspase (YCA1) [17,18] provided a structural basis for comparing caspases and metacaspases. The metacaspase structures revealed a monomeric enzyme containing a core caspase/haemoglobinase fold [19] with an eight-stranded β-sheet consisting of six parallel and two anti-parallel strands. This is unlike the caspases, which comprise a six-stranded β-sheet and a stable dimerization interface which forms the active enzyme. In addition, the recent structure of a paracaspase [20] shows that it is structurally very similar to the caspases and dimerizes in a similar manner. Conversely, the two extra strands in the β-sheet of the metacaspases prevent such dimerization, explaining its monomeric peptidase activity and distinguishing the metacaspases structurally from other caspase family members.

The high resolution crystal structure of TbMCA2 was determined using inactive mutants (TbMCA2 C213A/G), as autoprocessing of the full-length recombinant enzyme *in vitro* was unfavourable for producing diffraction quality crystals [17,18]. This revealed an unusual N-terminal region, which encircled the protein and crossed over the active site, blocking the S_1 pocket. Consequently, the structure of TbMCA2 does not contain an active site substrate and the properties of its extended binding site have not yet been established.

In this study, we undertook to examine the extended substrate specificity of recombinant and active TbMCA2 using a series of fluorescence resonance energy transfer (FRET) peptides. The specificity of TbMCA2 subsites S_3 to S_3' were analysed by kinetic assays that monitored the hydrolysis of a FRET peptide series where positions P_3 to P'_3 on the peptides are substituted by each of the natural amino acids. In addition, the effects of Ca^{2+} on the structure, activity and extended subsite specificity of TbMCA2 were investigated using a series of kinetic assays, intrinsic fluorescence analysis and circular dichroism spectroscopy.

Results

Effects of temperature, pH and Ca^{2+} concentration on the activity of TbMCA2

The activity of TbMCA2 was initially assayed using the reference substrate Abz-KARSSAQ-EDDnp over a range of temperatures (20–37 °C), pH values (pH 5 to pH 11) and $CaCl_2$ concentrations (0–5 mM).

Aliquots of TbMCA2 were incubated in the presence of Ca^{2+} at four different temperatures (20, 25, 30 and 37 °C) for 15 min and the residual activity was measured at 2.5 min and then at 5 min intervals showing that the remaining activity of TbMCA2 decreases most rapidly at higher temperatures (Fig. 1). At higher temperatures TbMCA2 undergoes much more extensive autoprocessing, as observed by SDS/PAGE analysis (data not shown), suggesting that while minimal autoprocessing is not detrimental [9], unlimited autoprocessing will ultimately inactivate TbMCA2. It was also noted that TbMCA2 is stable at 37 °C for at least 60 min when incubated in the presence of a saturating substrate concentration (data not shown). However, in order to reduce TbMCA2 activity loss during the reactions all assays were conducted at 25 °C.

The relationship between pH and k_{cat}/K_M, for the hydrolysis of Abz-KARSSAQ-EDDnp by TbMCA2, indicates an optimum pH for TbMCA2 activity of 7.7 and the participation of two ionizing groups with $pK_{e1} = 6.70 \pm 0.02$ and $pK_{e2} = 8.70 \pm 0.02$, which can be directly attributed to the histidine (pK_a 6.7)–cysteine (pK_a 8.7) catalytic dyad (Fig. 2). This bell-shaped pH profile and the calculated pK values are similar to those

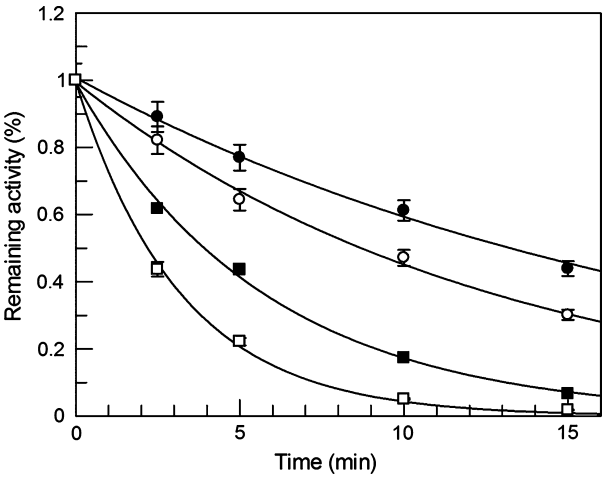

Fig. 1. The thermal stability of TbMCA2. The activity of TbMCA2 was measured over a 15-min period using time intervals of between 2.5 and 5 min at 37 °C (□), 30 °C (■), 25 °C (○) and 20 °C (●).

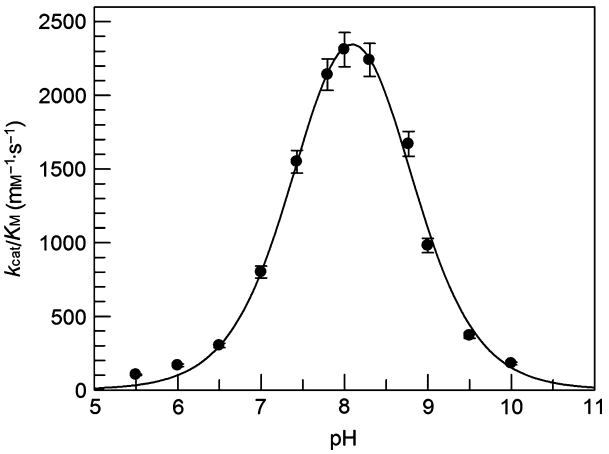

Fig. 2. The pH dependence of TbMCA2. The profile of k_{cat}/K_M for TbMCA2 hydrolysis of Abz-KARSSAQ-EDDnp indicates an optimum pH for activity of 7.7 and the participation of two ionizing groups with $pK_{e1} \sim 6.70$ and $pK_{e2} \sim 8.70$.

observed for caspases [21,22] indicating that TbMCA2 shares a similar pH dependence and signifies the existence of one active form of the enzyme with the increase in activity most probably a result of the de-protonation of the catalytic cysteine [22]. Such interpretation is supported by previous site directed mutagenesis studies [9] and more recently by the analysis of the crystallographic structure of TbMCA2 where the position of the Cys213Ala and His158 catalytic dyad was shown to be conserved with the caspases [17].

To investigate the effect of Ca^{2+} on the activity of TbMCA2, the kinetic parameters for the hydrolysis of Abz-KARSSAQ-EDDnp were calculated using $CaCl_2$ concentrations in the range 0–5 mM. Both k_{cat} and k_{cat}/K_M were found to increase sharply up to ~ 500 μM of $CaCl_2$ but above this concentration both k_{cat} and k_{cat}/K_M started to decrease (Fig. 3A,B). K_M increases with $CaCl_2$ concentration up to 1 mM and reaches a plateau above this $CaCl_2$ concentration (Fig. 3C). The fact that high $CaCl_2$ concentrations affect TbMCA2 efficiency and turnover but not substrate affinity suggests that, at high concentrations, $CaCl_2$ does not alter the substrate binding site.

TbMCA2 substrate specificity

The substrate specificity of TbMCA2 was studied using six individual series of FRET peptides derived from Abz-KARSSA-Q-EDDnp (Table 1). This peptide was chosen from a series of fluorogenic peptidase substrates that we had available in our laboratory and was modified in order to provide a simple and appropriate reference peptide for our work with TbMCA2. The peptides were synthesized by substituting a single amino acid residue in the Lys-Ala-Arg-Ser-Ser-Ala (KARSSA) portion of the substrate by all of the natural amino acids (with exception of Cys and Trp) at positions P_3 to P'_3, with the Arg-Ser (R↓S) bond being the cleavage site unless otherwise indicated. Where peptide synthesis was successful, the peptides were assayed and the resulting kinetic constants are shown in Table 1. In addition, the products of hydrolysis of the cleaved peptides were analysed by HPLC coupled to an ion spray mass spectrometer in order to verify the cleavage site(s) in each substrate.

P_1 residue: hydrolysis of the Abz-KA**X**SSAQ-EDDnp series

The substrates with basic residues (**X** = Arg or Lys) in P_1 were the only peptides to be hydrolysed by TbMCA2 in this series and the cleavage was exclusively at peptide bond Arg-Ser and Lys-Ser, with a clear preference for the peptide containing Arg at the P_1 position. All other peptides tested were resistant to cleavage. These results confirm the previously described substrate specificity of TbMCA2 [9] and of other metacaspases [8,13,23]. Peptides in the series that

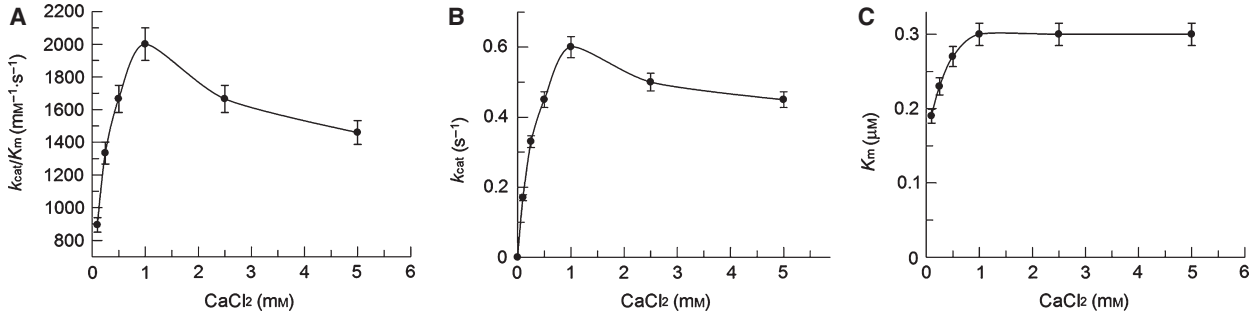

Fig. 3. Activity of TbMCA2 measured over a range of $CaCl_2$ concentrations. Kinetic parameters for the hydrolysis of Abz-KARSSAQ-EDDnp by TbMCA2 were calculated for k_{cat}/K_M (A), k_{cat} (B) and K_M (C).

Table 1. Kinetic parameters for the hydrolysis of FRET peptides derived from Abz-KARSSAQ-EDDnp by TbMCA2. An asterisk indicates the peptides that present substrate inhibition. The substrate inhibition parameters were calculated using Eqn (1). K_M, k_{cat} and k_{cat}/K_M are given here but the substrate inhibition constants (K_{iA}) are in the text. A dash represents peptides that were not assayed.

	Parameters	P_3 (K)	P_2 (A)	P_1 (R)	P′$_1$ (S)	P′$_2$ (S)	P′$_3$ (A)
R	K_M (μM)	0.37 ± 0.03	0.19 ± 0.01	0.29 ± 0.03	Cleavages R↓R and R↓S	Cleavage R↓S and R↓A	Cleavage R↓S and R↓Q
	k_{cat} (s^{-1})	0.500 ± 0.003	0.400 ± 0.005	0.600 ± 0.009			
	k_{cat}/K_M ($mM^{-1}·s^{-1}$)	1351	2105	2068			
K	K_M (μM)	0.29 ± 0.03	0.29 ± 0.02	0.49 ± 0.02	Cleavage R↓K and K↓S	Cleavage R↓S and K↓A	Cleavage R↓S and K↓Q
	k_{cat} (s^{-1})	0.600 ± 0.009	1.80 ± 0.03	0.300 ± 0.005			
	k_{cat}/K_M ($mM^{-1}·s^{-1}$)	2068	6206	612			
G	K_M (μM)	–	0.74 ± 0.08		2.2 ± 0.2	1.51 ± 0.06	0.30 ± 0.02
	k_{cat} (s^{-1})	–	0.300 ± 0.008	Resistant	0.100 ± 0.004	1.60 ± 0.02	0.100 ± 0.001
	k_{cat}/K_M ($mM^{-1}·s^{-1}$)	–	405	K_i = 17 μM	45	1059	333
A	K_M (μM)	–	0.29 ± 0.03		0.87 ± 0.07	–	0.29 ± 0.03
	k_{cat} (s^{-1})	–	0.600 ± 0.009	Resistant	0.500 ± 0.009	–	0.600 ± 0.009
	k_{cat}/K_M ($mM^{-1}·s^{-1}$)	–	2068	K_i = 7.5 μM	574	–	2068
L	K_M (μM)	0.85 ± 0.06	0.49 ± 0.06		1.4 ± 0.7	–	–
	k_{cat} (s^{-1})	0.300 ± 0.006	0.300 ± 0.007	Resistant	0.080 ± 0.004	–	–
	k_{cat}/K_M ($mM^{-1}·s^{-1}$)	352	612	K_i = 9.4 μM	57	–	–
I	K_M (μM)	–	0.56 ± 0.06			0.12 ± 0.01	3.2* ± 0.3
	k_{cat} (s^{-1})	–	0.0500 ± 0.0001	Resistant	Resistant	0.80 ± 0.01	2.9* ± 0.1
	k_{cat}/K_M ($mM^{-1}·s^{-1}$)	–	89	K_i = 4.8 μM	K_i = 7.8 μM	6666	906*
V	K_M (μM)	1.2 ± 0.1	1.2 ± 0.1		0.53 ± 0.04	0.36 ± 0.02	1.0 ± 0.1
	k_{cat} (s^{-1})	0.200 ± 0.003	0.40 ± 0.01	Resistant	0.050 ± 0.001	0.500 ± 0.007	1.90 ± 0.05
	k_{cat}/K_M ($mM^{-1}·s^{-1}$)	167	333	K_i = 8.4 μM	94	1388	1900
M	K_M (μM)	0.61 ± 0.04	0.2 ± 0.1		0.96 ± 0.02	–	0.36 ± 0.03
	k_{cat} (s^{-1})	0.200 ± 0.002	0.100 ± 0.003	Resistant	0.200 ± 0.005	–	0.400 ± 0.008
	k_{cat}/K_M ($mM^{-1}·s^{-1}$)	327	500	K_i = 12.4 μM	208	–	1111
P	K_M (μM)	–	0.83 ± 0.07			0.45 ± 0.04*	1.0 ± 0.1
	k_{cat} (s^{-1})	–	0.400 ± 0.009	Resistant	Resistant	0.100 ± 0.005*	0.300 ± 0.008
	k_{cat}/K_M ($mM^{-1}·s^{-1}$)	–	481	K_i = 9.4 μM	K_i = 4.6 μM	222*	300
F	K_M (μM)	0.33 ± 0.03	0.22* ± 0.01				0.64* ± 0.06
	k_{cat} (s^{-1})	0.100 ± 0.002	0.20* ± 0.01	Resistant	Resistant	Resistant	6.0* ± 0.3
	k_{cat}/K_M ($mM^{-1}·s^{-1}$)	303	909*	K_i = 4.2 μM	K_i = 3.9 μM	K_i = 9.6 μM	9375*
Y	K_M (μM)	–	0.22* ± 0.01				0.35 ± 0.03
	k_{cat} (s^{-1})	–	0.30* ± 0.01	Resistant	Resistant	Resistant	0.70 ± 0.02
	k_{cat}/K_M ($mM^{-1}·s^{-1}$)	–	1363*	K_i = 3.8 μM	K_i = 4.1 μM	K_i = 6.7 μM	2000
H	K_M (μM)	1.22 ± 0.01	0.72 ± 0.07		1.70 ± 0.06	0.29 ± 0.02	0.59 ± 0.04
	k_{cat} (s^{-1})	0.600 ± 0.002	0.300 ± 0.008	Resistant	0.300 ± 0.003	0.100 ± 0.005	0.80 ± 0.01
	k_{cat}/K_M ($mM^{-1}·s^{-1}$)	491	417	K_i = 5.1 μM	176	344	1355
N	K_M (μM)	2.1 ± 0.3	0.46 ± 0.03		1.6 ± 0.1	–	1.1 ± 0.1
	k_{cat} (s^{-1})	0.100 ± 0.004	0.400 ± 0.007	Resistant	0.40 ± 0.01	–	0.30 ± 0.01
	k_{cat}/K_M ($mM^{-1}·s^{-1}$)	48	869	K_i = 6.7 μM	250	–	272
Q	K_M (μM)	–	3.4 ± 0.2		1.38 ± 0.03	0.71 ± 0.04	0.50 ± 0.03
	k_{cat} (s^{-1})	–	0.90 ± 0.02	Resistant	0.300 ± 0.001	0.100 ± 0.001	0.200 ± 0.003
	k_{cat}/K_M ($mM^{-1}·s^{-1}$)	–	265	K_i = 5.7 μM	217	140	400
S	K_M (μM)	–	0.51 ± 0.05		0.29 ± 0.03	0.29 ± 0.03	1.6 ± 0.1
	k_{cat} (s^{-1})	–	0.200 ± 0.004	Resistant	0.600 ± 0.009	0.600 ± 0.009	0.80 ± 0.01
	k_{cat}/K_M ($mM^{-1}·s^{-1}$)	–	392	K_i = 7.8 μM	2068	2068	500
T	K_M (μM)	2.5 ± 0.2	1.0 ± 0.1		1.03 ± 0.06	–	1.9 ± 0.2
	k_{cat} (s^{-1})	0.200 ± 0.001	0.40 ± 0.02	Resistant	0.400 ± 0.005	–	0.20 ± 0.01
	k_{cat}/K_M ($mM^{-1}·s^{-1}$)	167	400	K_i = 9.4 μM	388	–	105
D	K_M (μM)		11.9 ± 1.7		2.9 ± 0.1	0.52 ± 0.05	4.0 ± 0.3
	k_{cat} (s^{-1})	Resistant	0.100 ± 0.005	Resistant	0.100 ± 0.005	0.080 ± 0.001	0.40 ± 0.01
	k_{cat}/K_M ($mM^{-1}·s^{-1}$)	K_i = 4.2 μM	8	K_i = 2.9 μM	34	153	100
E	K_M (μM)				2.1 ± 0.3	0.25 ± 0.04	0.44 ± 0.05
	k_{cat} (s^{-1})	Resistant	Resistant	Resistant	0.100 ± 0.005	0.60 ± 0.02	0.040 ± 0.001
	k_{cat}/K_M ($mM^{-1}·s^{-1}$)	K_i = 3.8 μM	K_i = 7.8 μM	K_i = 3.5 μM	48	2400	90

were found to be resistant to hydrolysis by TbMCA2 (where **X** ≠ Arg or Lys) were all assayed as inhibitors and found to be competitive inhibitors, for which the K_i values are shown in Table 1. It should be noted that lower K_i values were obtained with Abz-KA**D**S-SAQ-EDDnp or Abz-KA**E**SSAQ-EDDnp, indicating that the negatively charged side chain of Asp or Glu interacted with TbMCA2 in an unusual inhibitory manner, such as through allostery.

P_2 residue: hydrolysis of the Abz-K**X**RSSAQ-EDDnp series

Peptides containing basic amino acids Arg or Lys showed the highest specificity constants in this series (k_{cat}/K_M = 6200 $mM^{-1}\cdot s^{-1}$ and 2100 $mM^{-1}\cdot s^{-1}$, respectively), although the substrate containing an Ala substitution was also efficiently hydrolysed by TbMCA2 with k_{cat}/K_M = 2100 $mM^{-1}\cdot s^{-1}$. Peptides containing aromatic residues (Phe and Tyr) were also efficiently hydrolysed with k_{cat}/K_M = 1400 $mM^{-1}\cdot s^{-1}$ and 900 $mM^{-1}\cdot s^{-1}$, respectively, but these FRET peptides exhibited substrate inhibition at concentrations higher than 10 μM and the observed K_{iA} constants determined for the unproductive binding were 14.7 μM (Tyr) and 27.1 μM (Phe). The peptide that contained Asp at the P_2 position had the lowest k_{cat}/K_M value (8 $mM^{-1}\cdot s^{-1}$) and highest K_M (12 μM) and the peptide Abz-K**E**R-SSAQ-EDDnp was resistant to hydrolysis; thus a negatively charged group at the P_2 position of the substrates is very unfavourable for TbMCA2 activity.

P_3 residue: hydrolysis of the Abz-**X**ARSSAQ-EDDnp series

Of the peptides tested in this series, the substrates containing basic residues Arg or Lys at the P_3 position were the most susceptible to hydrolysis by TbMCA2. Together with the results for the P_2 series, this suggests a preference of TbMCA2 non-prime sites for positively charged basic residues. In accordance with this observation, the peptides containing Glu and Asp were resistant to hydrolysis but inhibited the enzyme with a K_i of around 4 μM. All the other peptides tested in this series were hydrolysed but with low k_{cat}/K_M.

P'_1 residue: hydrolysis of the Abz-KAR**X**SAQ-EDDnp series

All the peptides in this series susceptible to hydrolysis were cleaved at the Arg-X peptide bond except for the substrates where **X** = Arg or Lys; these substrates were also hydrolysed by TbMCA2 at the Arg-Arg (or Arg-Lys) (60%) and Arg-Ser (or Lys-Ser) (40%) positions. The kinetic parameters for peptides hydrolysed at more than one position were not calculated. The reference peptide with Ser at the P'_1 position was the most susceptible substrate to hydrolysis by TbMCA2 (k_{cat}/K_M = 2100 $mM^{-1}\cdot s^{-1}$), while peptides containing aliphatic residues were poorly hydrolysed or even resistant to hydrolysis (Pro and Ile). In addition, TbMCA2 did not cleave peptides containing the aromatic residues Phe and Tyr at this position, and those with negatively charged side chains (Asp and Glu) were poorly hydrolysed. These results suggest that the S'_1 binding pocket has a preference for residues with small side chains.

P'_2 residue: hydrolysis of the Abz-KARS**X**AQ-EDDnp series

Of the substrates tested in this series, the one that was most susceptible to hydrolysis by TbMCA2 was the peptide containing Ile at the P'_2 position. The peptide containing Glu at this position was also well hydrolysed by TbMCA2, with k_{cat}/K_M = 2400 $mM^{-1}\cdot s^{-1}$; however, this contrasts sharply with the low hydrolysis observed when an Asp is present in P'_2 (k_{cat}/K_M = 153 $mM^{-1}\cdot s^{-1}$). The substrate containing Pro in P'_2 presented substrate inhibition and the estimated inhibition constant for this unproductive enzyme–substrate interaction is K_{iA} = 5.9 μM. In addition, peptides with Ser, Gly or Val at this position were hydrolysed with relatively high k_{cat}/K_M values, whereas peptides with the aromatic residues Tyr and Phe were resistant to hydrolysis.

P'_3 residue: hydrolysis of the Abz-KARSS**X**Q-EDDnp series

In this series, the peptide containing Phe at the P'_3 position showed the highest k_{cat}/K_M (9375 $mM^{-1}\cdot s^{-1}$) amongst all of the assayed peptides, mainly due to the high value of k_{cat} (6.0 s^{-1}), but this substrate also showed substrate inhibition kinetics with K_{iA} = 3.7 μM. TbMCA2 also efficiently hydrolysed the peptide containing Tyr at the P'_3 position; however, this happened without substrate inhibition. Peptides with Ala, Ile, His and Met were also efficiently hydrolysed by TbMCA2 ($k_{cat}/K_M \geq 900$) with the peptide containing Ile also displaying substrate inhibition (K_{iA} = 0.5 μM).

Influence of $CaCl_2$ on TbMCA2

The effects of Ca^{2+} on the activity of TbMCA2 were further investigated using the fluorogenic peptides

Z-RR-AMC and Z-FR-AMC, which are both hydrolysed at Arg↓AMC. Different profiles of activation were observed for these two substrates: the hydrolysis of Z-RR-AMC produced a k_{cat}/K_M that significantly increased up to a concentration of 250 μM $CaCl_2$ and then decreased at higher concentrations, whereas the k_{cat}/K_M values of Z-FR-AMC increased until around 6 mM $CaCl_2$ and declined after this (to the measured 20 mM) (Fig. 4A). As these two peptides differ only at the P_2 position, the influence of this residue on the activation of TbMCA2 by Ca^{2+} was further explored.

Initially, the FRET peptides Abz-K**R**R↓SSAQ-EDDnp, Abz-K**F**R↓SSAQ-EDDnp and Abz-K**A**R↓SSAQ-EDDnp were assayed over a range of Ca^{2+} concentrations (0–5 mM) and the activation profiles for the hydrolysis of these longer peptides were found to be similar to those observed with Z-RR-AMC and Z-FR-AMC (Fig. 4B). This confirmed that the P_2 residue had an effect on the activation of TbMCA2 by Ca^{2+}.

To confirm these results the effect of Ca^{2+} concentration on the kinetic behaviour of TbMCA2 was tested with all substrates presented in Table 1. Kinetic assays were carried out with TbMCA2 using the series of peptides at low (50 μM) and high (1 mM) Ca^{2+} concentrations but only substrates with residues that varied in P_2 (P_2-varying substrates, Abz-K**X**RSSAQ-EDDnp) presented a differential Ca^{2+} effect as represented in Fig. 5 and Table 2. Analysing the results from these assays revealed that the P_2-varying substrates could be split into three distinct groups:

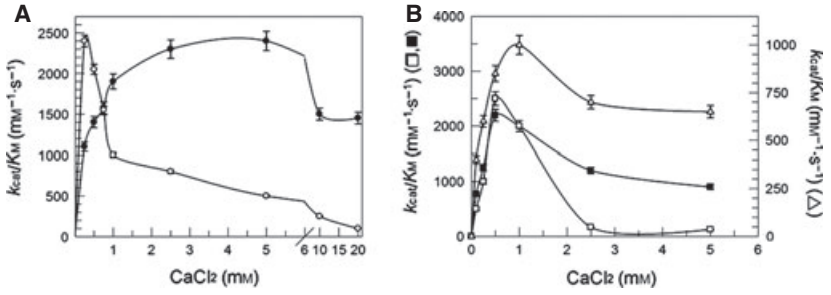

Fig. 4. The influence of $CaCl_2$ on TbMCA2 activity. (A) The effect of $CaCl_2$ on k_{cat}/K_M for the hydrolysis of Z-FR↓-AMC (●) and Z-RR↓-AMC (○) by TbMCA2. (B) The effect of $CaCl_2$ on k_{cat}/K_M for the hydrolysis of Abz-K**A**R↓SSAQ-EDDnp (■), Abz-K**R**R↓SSAQ-EDDnp (□) and Abz-K**F**R↓SSAQ-EDDnp (▵) by TbMCA2.

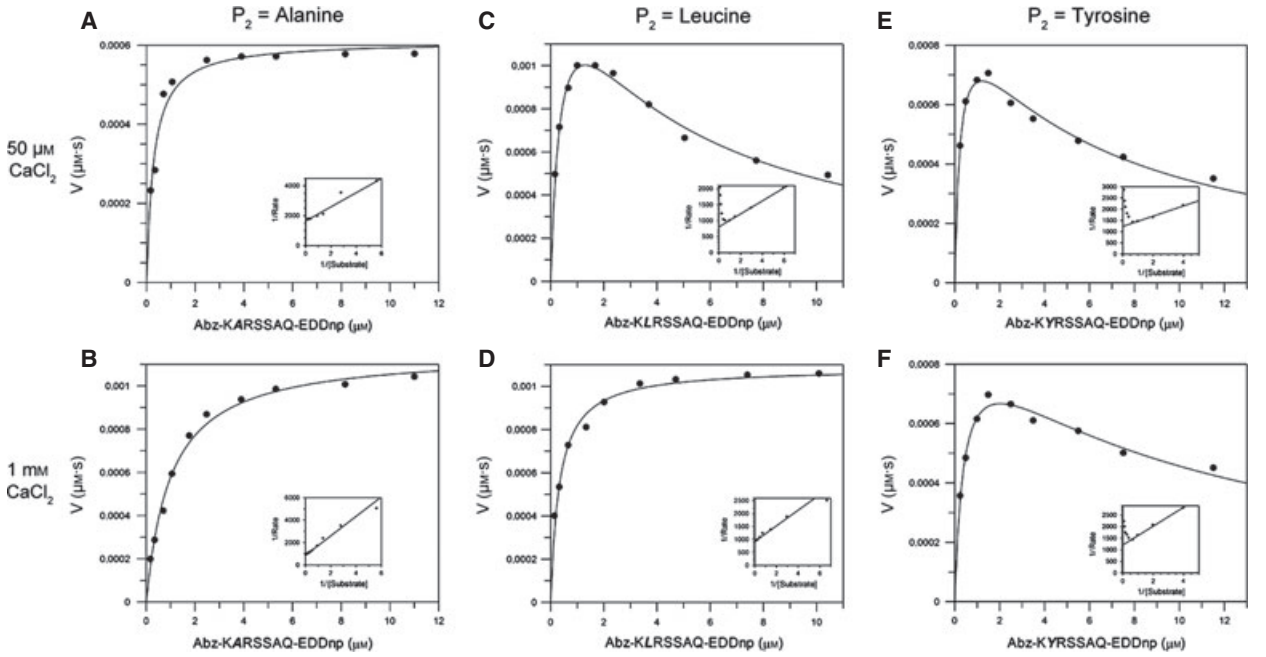

Fig. 5. Differential effect of calcium activation for substrates varying at the P_2 position. The hydrolysis rate of reaction versus substrate concentration was plotted in the presence of 50 μM (low) and 1 mM (high) $CaCl_2$ for FRET substrates that differed in the P_2 position. The representative substrates shown are Abz-K**A**R↓SSAQ-EDDnp [P_2 = Ala, (A) and (B)]; Abz-K**L**R↓SSAQ-EDDnp [P_2 = Leu, (C) and (D)] and Abz-K**Y**R↓SSAQ-EDDnp [P_2 = Tyr, (E) and (F)].

Table 2. Substrate inhibition constants (K_{iA}) determined at various calcium concentrations with the three representative substrates containing changes at the P_2 position. ND, not determined.

	K_{iA} (μM)		
$CaCl_2$ (μM)	Abz-K**A**RSSAQ-EDDnp	Abz-K**L**RSSAQ-EDDnp	Abz-K**Y**RSSAQ-EDDnp
50	ND	2.9 ± 0.1	6.4 ± 0.3
100	ND	4.8 ± 0.2	7.9 ± 0.4
250	ND	12.3 ± 0.6	9.4 ± 0.4
500	ND	28.6 ± 1.4	7.3 ± 0.4
750	ND	ND	10.9 ± 0.5
1000	ND	ND	14.7 ± 0.6
2000	ND	ND	11.0 ± 0.5
5000	ND	ND	12.4 ± 0.6

substrates that show no inhibition regardless of the Ca^{2+} concentration (Ala, Thr and Gly); substrates that show inhibition at low (50 μM) but not high (1 mM) Ca^{2+} concentrations (Leu, Ile and Gln); and substrates that inhibit TbMCA2 regardless of the Ca^{2+} concentration (Tyr and Phe). These differential Ca^{2+} effects are exemplified using a representative substrate from each group (Ala, Leu and Tyr) by plotting substrate hydrolysis velocity (V) versus substrate concentration [S] at both low (50 μM) and high (1 mM) Ca^{2+} concentrations and by calculating the substrate inhibition constants K_{iA} over a range of Ca^{2+} concentrations (Fig. 5 and Table 2, respectively).

Kinetic assays using substrates represented by Ala at the P_2 position produced hyperbolic plots at both low (50 μM) and high (1 mM) Ca^{2+} concentrations (Fig. 5A,B) and showed no substrate inhibition (Table 2). However, for peptides represented by Leu in P_2, the kinetics for hydrolysis presented substrate inhibition at low Ca^{2+} concentration (50 μM) which was completely abolished in assays performed in the presence of a high concentration of Ca^{2+} (1 mM) (Fig. 5C, D). This effect was shown to be gradual, with the K_{iA} values rising with increasing Ca^{2+} concentration until around 0.5 mM after which substrate inhibition was abolished (Table 2). Additionally, kinetic assays performed with peptides represented by Tyr in P_2 showed that excess substrate inhibition kinetics were observed independent of the Ca^{2+} concentration, as shown in Fig. 5E,F and Table 2.

Examining Ca^{2+} binding in TbMCA2

It has been shown previously that the addition of Ca^{2+} to TbMCA2 activates the enzyme and leads to autoprocessing events [9]. To better understand how Ca^{2+} might activate TbMCA2, we analysed TbMCA2 using far-UV circular dichroism spectra and intrinsic fluorescence assays (Fig. 6). Prior to analysis, a sample of TbMCA2 was treated with 1 mM $CaCl_2$ and

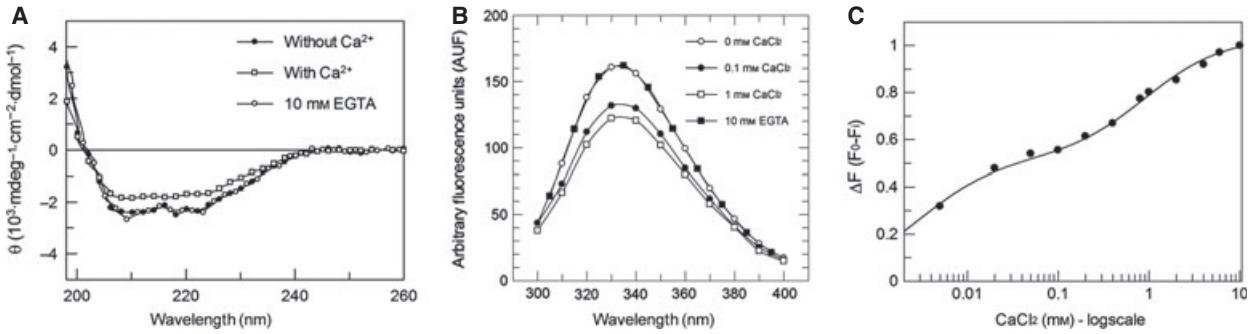

Fig. 6. The effect of $CaCl_2$ on the structure of TbMCA2. (A) Circular dichroism spectra of TbMCA2 in the absence (■) or in the presence (□) of 1 mM $CaCl_2$ or in the presence of 1 mM $CaCl_2$ plus 10 mM EGTA (○). Ellipticity is reported as mean residue molar ellipticity Θ (deg·cm^2·dmol^{-1}). (B) Fluorescence emission spectra of TbMCA2 (λ_{ex} = 280 nm) in the absence (■) or in the presence (□) of 1 mM $CaCl_2$ or in the presence of 1 mM $CaCl_2$ plus 10 mM EGTA (○). (C) Changes in the maximum fluorescence intensity at an emission wavelength of 330 nm upon increasing the $CaCl_2$ concentration (log scale).

peptidase activation was confirmed by visualizing the autoprocessing products on SDS/PAGE (data not shown). The far-UV circular dichroism spectra of TbMCA2 in the absence and presence of 1 mM $CaCl_2$ are shown in Fig. 6A and clearly show the secondary structure modification in the presence of Ca^{2+}. This effect was completely reversed by subsequent addition of 10 mM EGTA, indicating that TbMCA2 undergoes a reversible structural change on binding Ca^{2+}.

Intrinsic fluorescence emission spectra of TbMCA2 were measured in the absence of Ca^{2+} or in the presence of 10 mM EGTA, 0.1 mM $CaCl_2$ or 1 mM $CaCl_2$ (Fig. 6B). A shift in the intrinsic fluorescence of TbMCA2 was observed in the presence of Ca^{2+}, which was more pronounced at higher Ca^{2+} concentrations (Fig. 6B). When the intrinsic fluorescence was examined more closely and the shift in fluorescence was plotted against a range of Ca^{2+} concentrations (0–10 mM), the curve revealed two points of inflexion, consistent with the existence of two Ca^{2+} binding sites in TbMCA2 (Fig. 6C). Dissociation constants (K_D) for these two sites were calculated using the Adair equation giving $K_{D1} = 3.0 \pm 0.3$ μM and $K_{D2} = 900 \pm 100$ μM. Data fitting could only be obtained using $n = 2$ (two binding sites), confirming the visual observation of two points of inflexion.

Docking of VRPR into the active site of TbMCA2

Docking studies of VRPR into the active site of TbMCA2, lacking five N-terminal residues, resulted in the ligand binding in several conformations all of which had similar predicted binding affinities. However, a 3D alignment of TbMCA2 with the structures from other clan CD [2] members revealed that the position of the catalytic dyad is conserved between all structures in the family [17]. In addition, where these structures have been determined with inhibitors bound in their active sites (caspase-7, PDB ID 1F1J [24]; paracaspase, PDB ID 3UOA [20]; gingipain-R, PDB ID 1CVR [25] and MARTX toxin, PDB ID 3GCD [26]), the orientation of the ligand and the position of the P_1 residue are all consistent (data not shown). Consequently, from the docking results, a conformation of VRPR in the active site of TbMCA2 was chosen that bound to the enzyme in a similar manner to other clan CD members.

VRPR docked into the crystal structure of TbMCA2 revealed that the P_1 Arg of VRPR binds in the predicted, acidic S_1 binding pocket of TbMCA2 with its carbonyl oxygen situated between the catalytic dyad (Fig. 7). It does this by forming hydrogen bonds, via its guanidinium group, to the carboxylic acid groups

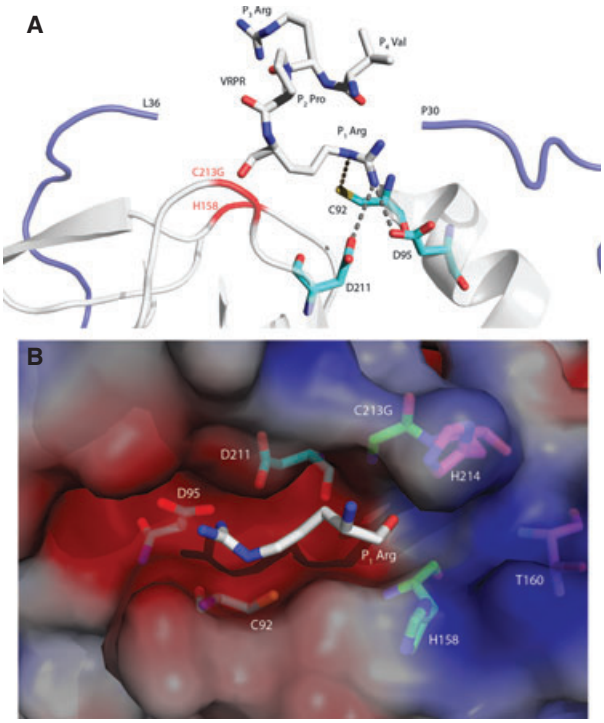

Fig. 7. Docking of VRPR into the active site of $TbMCA2^{C213G}$ lacking the N-terminal residues 31–35 ($TbMCA2^{t}$). (A) Docked VRPR interacts with residues in the S_1 binding pocket (cyan) and sits in the path of the deleted N-terminal region of TbMCA2 (blue). (B) The docked P_1 Arg of VRPR sits in the acidic S_1 binding pocket (including residues C92, D95, D211), sandwiched between the catalytic dyad (C213G and H158) with the prime side of the ligand situated near a narrow channel that includes residues H214 and T160. The electrostatic surface potential of $TbMCA2^{t}$ was calculated with APBS [42] contoured at ± 3 *kT*/*e* and shows the positively (blue) and negatively (red) charged surface areas. Structural figures were prepared using PYMOL [43].

of Asp95 and Asp211 (Fig. 7A). Cys92 also sits within hydrogen bonding distance of the functional group on the P_1 Arg (Fig. 7A) and the prime side of the bound ligand sits at a narrow channel formed by His214 and Thr160 (Fig. 7B).

The docked VRPR sits at a position previously occupied by residues 31–34 (protein sequence YLVQ) in the N-terminal domain of TbMCA2 (Fig. 7A). These residues, along with residues at the C-terminal end of the partially disordered 280-loop and on an ordered loop between strand β1 and helix α1 in TbMCA2 (residues 270–280 (sequence ATFGST GSTGA) and 86–91 (sequence SAALSG), respectively [17]), are the only areas of TbMCA2 that surround the bound ligand and consequently are the most likely to be involved in forming the S_2–S_3 binding pockets.

Discussion

Using a series of peptide substrates spanning the residues P_3–P'_3 of a TbMCA2 substrate, we have unequivocally demonstrated that TbMCA2 has a strict preference for basic charged amino acids (Arg or Lys) at the P_1 position, with a preference for Arg. Similar specificity occurs in metacaspases from other organisms [8,13,23]. The 3D crystal structure of TbMCA2 revealed that the basis for this strict specificity results from its S_1 subsite being a negatively charged pocket lined by the functional groups of residues Cys92, Ser156, Asp95 and Asp211 [17]. To demonstrate how a substrate with Arg at the P_1 position might bind in the S_1 pocket of TbMCA2 we docked the peptide VRPR into the active site of TbMCA2 (Fig. 7). This revealed that the ligand bound to the active site through its P_1 Arg forming hydrogen bonds to Asp95 and Asp211 (Fig. 7B), which were previously shown to be essential for TbMCA2 activity [17].

In addition to the clear specificity of TbMCA2 for Arg or Lys in P_1, it has also been shown that TbMCA2 shows a preference for peptides containing basic amino acids at the non-prime side (P_2 and P_3). This was also shown for the P_3 position for substrates of *Arabidopsis thaliana* metacaspase 9 (AtMCA9) where V**R**PR-AMC was identified as an optimized substrate [27], and the k_{cat}/K_M values for TbMCA2 (Table 1) suggest that, from this series of peptides, Abz- KKRSSA-EDDnp is one of the most effective substrates for the enzyme. Furthermore, peptides containing negatively charged residues Asp and Glu at the P_2 and P_3 positions were resistant to hydrolysis by TbMCA2. This result appears to be different in protein substrates, where autoprocessing in TbMCA2 was found to occur at sites where Asp residues occupy the P_3 positions [9]. This is presumably due to the differences found in cleaving a large protein substrate as opposed a small peptide, the character of which will be dominated by the small number of residues present. In addition, results from the docking studies of VRPR into the active site of TbMCA2 suggest that the regions most likely to form the S_2 and S_3 subsites are reasonably hydrophobic but interspersed with several polar residues (Ser, Thr and Gln). This suggests that, even in the absence of highly acidic or basic functional residues lining the S_2 and S_3 pockets of TbMCA2, the enzyme specializes in, and has a preference for, basic substrates and that negatively charged residues, at least on a small peptide, will interfere with its mechanism.

Peptides in our study containing non-basic residues at P_1 were found to be competitive inhibitors of TbMCA2. As the S_1 binding pocket has been shown to be negatively charged (Fig. 7A and [17]) and is almost certainly structured to be highly specific in accepting basic P_1 residues, it is most likely that these peptides are involved in binding to an allosteric subsite which subsequently prevents substrate binding to the active site.

Substrate inhibition kinetics were also observed for several other peptides in the series, perhaps most notably for substrates with aromatic residues (Phe and Tyr) at positions P'_1 and P'_2. These peptides were resistant to cleavage by TbMCA2 and their ability to function as competitive inhibitors suggests that aromatic residues in these positions would also result in the substrate being involved in an alternative mode of allosteric binding. In addition, kinetic assays for the P'_1 series suggested that the S'_1 binding pocket may favour residues with small side chains. This is also confirmed by the maximum efficiency of TBMCA2, against this series of FRET peptides, being achieved with the substrate k_{cat}/K_M Abz- KARSIA–EDDnp. This can be further explained by examining the position of the prime side of the docked VRPR in the structure of TbMCA2 (Fig. 7A) where a residue at this position would sit near to the small groove in the protein that would occlude larger aromatic side chains. In addition, FRET peptides containing basic amino acids at the prime side of the P_1 Arg resulted in a second cleavage site by TbMCA2, which meant that the resulting kinetic parameters could not be calculated. However, these additional cleavage sites were not observed in assayed peptides that contained the P_1 Arg along with basic residues at positions P_2 or P_3. This shows that it is important for TbMCA2 to form interactions in its extended active site in order to execute substrate hydrolysis.

TbMCA2 is dependent on Ca^{2+} for activation [9] and the kinetic behaviour of TbMCA2 tested using the entire series of FRET peptides revealed that the concentration of Ca^{2+} had a differential effect on the activity of TbMCA2 only when the series of peptides that differed in P_2 were used. In this series it was found that both the type of residue at P_2 and the concentration of Ca^{2+} used could affect the activity of TbMCA2 (Fig. 4, 5 and Table 2). These results suggest that the substrate inhibition exhibited by these peptides occurs in the vicinity of and/or via a Ca^{2+} binding site in TbMCA2 and that general allosteric inhibition may occur by preventing Ca^{2+} binding to the correct site(s) in the enzyme. In addition, the change in the far-UV circular dichroism spectra of TbMCA2 in the presence of 1 mM $CaCl_2$ demonstrated that Ca^{2+} binding to the enzyme causes

a reversible structural modification. These data were backed up by intrinsic fluorescence assays, performed in the presence of various Ca^{2+} concentrations, which also indicated a structural shift on Ca^{2+} binding and the presence of at least two Ca^{2+} binding sites in TbMCA2. One of the binding sites was shown to have a high affinity for Ca^{2+} (K_{D1} = 3.0 ± 0.3 μM) while the other had a much lower affinity (K_{D2} = 900 ± 100 μM).

Structural studies on (an inactive mutant of) TbMCA2 identified a single Ca^{2+} binding site on the surface of the protein (residues Asp173, Asp189, Asp190 and Asp220), which was shown to be essential for both the activity of the enzyme and inhibitor binding [17] and is assumed to be the high affinity Ca^{2+} binding site identified in this study. This site is found at a location distinct from the active site and substrate binding pocket of TbMCA2 and the available structural data suggest that Ca^{2+} binding this site would not have a direct effect on the conformation of TbMCA2. Despite a thorough search for Ca^{2+} binding sites in TbMCA2 crystals, none was identified. However, TbMCA2 crystals that were soaked in various concentrations of $CaCl_2$ showed a large conformational change in a loop that is positioned near to the predicted substrate binding pocket (denoted the 280-loop) [17]. In the absence of bound substrate the 280-loop was highly disordered in the crystal structures and it is assumed that the low affinity Ca^{2+} binding site and the conformational changes observed, using far-UV circular dichroism and intrinsic fluorescence emission spectra, can be attributed to movement in this region.

In this study we have shown that peptides that are resistant to cleavage can act as inhibitors of TbMCA2. TbMCA2 has a highly specific P_1 substrate binding pocket and consequently the mechanism of inhibition must be allosteric. In addition, certain substrates (e.g. FRET substrates with Leu in P_2) were found to inhibit TbMCA2 at low concentrations of Ca^{2+} but not at high, which suggests that the allosteric inhibition of TbMCA2 is most likely to occur around the high affinity Ca^{2+} binding site. In these cases, the substrate is assumed to be binding to both the active and the allosteric site at low Ca^{2+} concentrations and as the concentration of Ca^{2+} increases the substrate is displaced from the high affinity Ca^{2+} binding site allowing the enzyme to retain full activity.

In another family of well-characterized calcium-dependent proteases, the calpains, a two-stage activation mechanism is governed by two different types of Ca^{2+} binding [28]. In view of our data, it seems possible that a similar bi-modal Ca^{2+}-dependent mechanism could operate in TbMCA2. In the parasite, TbMCA2 is found to reside mainly in the RAB11-positive endosomes [7] where the basal level of Ca^{2+} is reported to be ~ 100 nM [29]. This is 30 times lower than the calculated K_{D1} (3.0 ± 0.3 μM) leading to the supposition that under regular conditions TbMCA2 is inactive. This phenomenon was also observed in the calpains where the levels of Ca^{2+} required to activate the enzymes were much higher *in vitro* than those measured intracellular, leading to the hypothesis that certain cellular associations or events could lower the Ca^{2+} activation threshold [30]. Consequently, we assume that *in vivo* TbMCA2 will be activated in response to certain cellular stimuli that will either raise the Ca^{2+} levels or lower the Ca^{2+} activation threshold in order to occupy both Ca^{2+} binding sites, and thus intracellular Ca^{2+} levels will be used to control the physiological function of MCA2 [9]. The Ca^{2+} dependence of TbMCA2 (and presumably the other metacaspases) is key to unravelling the role of these proteases.

Overall, this work has investigated the substrate specificity of TbMCA2 from S_3 to S'_3 using a new series of FRET substrates and the docking studies of VRPR into the active site of the enzyme. As no *in vivo* substrate for trypanosome MCA2 has been identified to date, these studies provide insights into the properties of potential TbMCA2 substrates. They also demonstrate the importance of the calcium ion for TbMCA2 activity, revealing a reversible structural modification on Ca^{2+} binding and the presence of a high and low affinity binding site. Furthermore, this work revealed that FRET peptides that were resistant to hydrolysis by TbMCA2 acted as competitive inhibitors and that substrates that differed in the P_2 position could produce differential Ca^{2+} effects on the activity of TbMCA2, suggesting that the enzyme is susceptible to allosteric inhibition via the high affinity Ca^{2+} binding site under certain conditions.

Experimental procedures

Expression of recombinant TbMCA2

The expression plasmid for recombinant TbMCA2 with an N-terminal His-tag has been described previously [9]. This plasmid was transformed into chemically competent *Escherichia coli* BL21 (DE3) pLysS cells (Novagen, Darmstast, Germany) and initially grown in 10 mL Luria broth medium supplemented with kanamycin (50 $\mu g \cdot mL^{-1}$), chloramphenicol (50 $\mu g \cdot mL^{-1}$) and glucose (5 mM) (supplemented LB, sLB) and incubated at 30 °C overnight (~ 16 h) with shaking at 150 r.p.m. The overnight cultures were

transferred to 1 L of sLB medium at 30 °C and grown until the culture density reached an A_{600} of 0.4. The temperature was reduced to 20 °C until the cell density reached an A_{600} of 0.6–0.7 and the bacterial cells were then harvested by centrifugation (4000 ***g*** for 10 min at 4 °C). Finally the cells were resuspended in 1 L of fresh sLB medium (without glucose). At this point isopropyl-β-D-1-thiogalactopyranoside was added to a final concentration of 0.5 mM and the cells were incubated at 20 °C for 14–16 h before being harvested by centrifugation at 4000 ***g*** for 10 min at 4 °C. The pellet was subsequently stored at −70 °C until required.

Purification of recombinant TbMCA2

The cell pellet was resuspended in 20 mL of 50 mM sodium phosphate pH 8.0, 500 mM NaCl, 20 mM imidazole and 1 $mg{\cdot}mL^{-1}$ lysozyme and incubated on ice for 30 min before the addition of 5 $\mu g{\cdot}mL^{-1}$ RNase, 5 $\mu g{\cdot}mL^{-1}$ DNase and 0.02% Triton X-100. The solution was further incubated for 30 min on ice before centrifugation at 26 000 ***g*** for 20 min at 4 °C and the supernatant was recovered.

The supernatant from the cell lysis was loaded onto a 1 mL HisTrap Ni^{2+} Sepharose column (GE Healthcare, Amersham, UK) previously equilibrated in 20 mM sodium phosphate pH 8.0, 500 mM NaCl (binding buffer) using a flow rate of 0.5 $mL{\cdot}min^{-1}$. The column was then washed with 5 mL of binding buffer and recombinant TbMCA2 was purified and eluted using a step gradient consisting of 5 mL of 50, 100, 150 and 500 mM imidazole in the same buffer. Recombinant TbMCA2 was found to elute between 100 and 150 mM imidazole (as confirmed by SDS/PAGE analysis) and the fractions containing the protein were pooled. In order to desalt and further purify the sample, the pooled protein was loaded directly onto a Sephadex G-75 size-exclusion column, prepacked with 100 mL of resin (GE Healthcare) and equilibrated in 50 mM Tris pH 7.4, 150 mM NaCl (NaCl/Tris buffer). Elution fractions were analysed using SDS/PAGE and the fractions containing recombinant TbMCA2 were collected. The fractions containing pure, recombinant TbMCA2 were concentrated (~ 10-fold) using an Amicon filtration unit (Millipore Corp., Billerica, MA, USA) equipped with a 10 kDa exclusion membrane, and the recovered protein was stored in NaCl/Tris buffer at −70 °C. The working aliquots were diluted in NaCl/Tris buffer containing 30% glycerol and stored at −20 °C. Repeated freeze–thaw cycles can decrease TbMCA2 activity and were consequently avoided.

Peptide synthesis

FRET peptides of the type Abz-peptidyl-Gln-EDDnp, where Abz is the fluorescent group *ortho*-aminobenzoic acid and EDDnp is the C-terminal quencher moiety *N*-(2,4-dinitrophenyl)-ethylenediamine, were synthesized by solid-phase synthesis (as described in [31]) using a bench-top automated solid-phase peptide synthesizer (PSSM-8, Shimadzu, Tokyo, Japan). The molecular mass and purity of the peptides were checked by analytical HPLC (Shimadzu 10AVP HPCL system) and by MALDI-TOF MS using a microflex LT system (Bruker Daltonics, Bremen, Germany). Stock solutions of the peptide substrates were prepared in distilled water and the concentration was measured spectrophotometrically at 365 nm using the molar extinction coefficient of the Dnp group of 17 300 $M^{-1}{\cdot}cm^{-1}$.

Kinetic assays

The activity of TbMCA2 was monitored by measuring the release of fluorescent groups, Abz or AMC (7-amino-4-methoxy coumarin), from the hydrolysis of the FRET substrates Abz-peptidyl-Gln-EDDnp and benzyloxycarbonyl (Z)-peptidyl-AMC respectively by the enzyme. Measurements were made using a Shimadzu (Tokyo, Japan) RF-5301PC spectrofluorometer with the excitation and emission wavelengths set at 320 and 420 nm, respectively, for the hydrolysis of the FRET substrates and 380 and 460 nm, respectively, for the hydrolysis of the Z-peptidyl-AMC substrates.

A 1 cm path-length cuvette containing 1 mL of the substrate solution was placed in a thermostatically controlled cell compartment for 5 min before the enzyme solution was added, and TbMCA2 was pre-incubated with 2.5 mM dithiothreitol. The kinetic measurements of peptide hydrolysis were performed at 25 °C in 50 mM Tris/HCl pH 7.4, 100 mM NaCl, 1 mM $CaCl_2$, unless otherwise stated. The progress of the reaction was continuously monitored by the fluorescence of the released products. The rate of increase of fluorescence was converted into moles of hydrolysed substrate per second, based on the fluorescence curves of standard peptide solutions before and after total enzymatic hydrolysis.

The enzyme concentration for the initial rate determination was chosen at a level intended to hydrolyse < 5% of the substrate present. TbMCA2 concentrations varied from 1 nM to 100 nM and substrate concentrations were adjusted in order to obtain a $V \times$ [S] plot with minimum substrate concentration ranging from 0.1 K_M to 10 K_M. The inner filter effect was corrected for using an empirical equation which has been described previously [32]. Kinetic parameters (k_{cat}, K_M and k_{cat}/K_M) were calculated according to Wilkinson [33] and by the use of Eadie–Hofstee plots.

The kinetic parameters for the peptides that presented substrate inhibition kinetics were calculated using

$$V = V_{max}[S]/\{K_M + [S]/([S]/K_{iA})\} \quad (1)$$

where V is velocity, V_{max} is the maximum velocity, [S] is the substrate concentration, K_M is the Michaelis constant and K_{iA} is the substrate inhibition constant.

All of the data obtained were fitted to nonlinear least-squares equations, using GRAFIT5 (Erithacus Software [34]).

Determination of inhibition parameters

The substrate Abz-KARSSAQ-EDDnp was used as a reference substrate in the cleavage reactions with TbMCA2, and any derivatives of this that were found to be resistant to hydrolysis by TbMCA2 were assayed as competitive inhibitors. For these peptides the inhibition parameters were determined in a continuous assay using Z-FR-AMC as the substrate. The equation used to calculate K_i values was $K_i = K_{i,app}/(1 + [S]/K_M)$, where [S] is the molar concentration of the substrate, K_M is the Michaelis constant and $K_{i,app}$ is the apparent inhibition constant. $K_{i,app}$ was calculated using the equation $V_o/V_i = 1 + [I]/K_{i,app,}$ where V_0 is the velocity of hydrolysis without the inhibitor, V_i is the velocity of hydrolysis in the presence of the inhibitor and [I] is the molar concentration of the inhibitor. A plot of $(V_0/V_i) - 1$ versus [I] yields a slope of $1/K_{i,app}$ [35].

The pH dependence of the kinetic parameters

The k_{cat}/K_M parameters were determined in the pH range 5–10 using Abz-KARSSAQ-EDDnp as the substrate in a four-component buffer system of constant ionic strength (25 mM glycine, 25 mM acetic acid, 25 mM MES and 75 mM Tris). The kinetic data were analysed by nonlinear regression using GRAFIT5 software [34] and

$$k = k_{(limit)}[1/(1 + 10^{pK_1 - pH} + 10^{pH - pK_2})] \quad (2)$$

Equation (2) fits the data when the pH–activity profile depends upon two ionizing groups in a bell-shaped curve and the activities at low and high pH are zero. k(limit) corresponds to the pH-independent maximum rate constant, K_1 and K_2 are the dissociation constants of a catalytically competent base and acid, respectively, and $k = k_{cat}/K_M$ [35].

The effect of calcium on the intrinsic fluorescence of TbMCA2

Structural changes in TbMCA2 were studied by monitoring the intrinsic fluorescence in 50 mM Tris/HCl pH 7.4, 100 mM NaCl with the addition of varying concentrations of $CaCl_2$ (50 μM to 2 mM) and a final protein concentration of 2 μM. The emission spectra were collected in the range 300–400 nm at 25 °C using a fixed excitation wavelength of 280 nm (2.5 nm slit width for both excitation and emission). These data were analysed using the Adair equation that describes the binding of ligands to multiple sites on a receptor using GRAFIT5 software [34].

Circular dichroism

Circular dichroism spectra were recorded on a JascoJ-810 spectropolarimeter (Jasco, Easton, MD, USA) with a Peltier system for controlling cell temperature. The absorbance spectra of TbMCA2 (10 μM) were collected in the far-UV range (190–260 nm) using a 1 mm path-length cell. The system was routinely calibrated with an aqueous solution of twice crystallized d^{10}-camphorsulfonic acid. Ellipticity was recorded as the mean residue molar ellipticity Θ ($deg \cdot cm^2 \cdot dmol^{-1}$). The spectrometer conditions typically included a sensitivity of 100 mdeg, a resolution of 0.5 nm, a response time of 4 s and a scan rate of 20 $nm \cdot min^{-1}$, and each curve is an average of four sequential scans at 25 °C. The control baseline was obtained with all buffer components prepared without the protein.

Protein concentration

For circular dichroism, intrinsic fluorescence and kinetic assays the protein concentration was determined spectrophotometrically based on the absorbance at 280 nm and on the calculated molar extinction coefficient of 29 910 $M^{-1} \cdot cm^{-1}$ (as calculated by PROTPARAM [36]).

Determination of cleavage sites in the substrates

The scissile bonds of hydrolysed peptide substrates were identified by isolation of the fragments using analytical HPLC followed by determination of their molecular mass by liquid chromatography mass spectrometry using an LCMS-2010 EV mass spectrometer (Shimadzu) equipped with an electrospray ionization probe. For the substrates hydrolysed at two sites the percentage of each cleavage product was calculated from the individual integrated areas taken from the chromatograms.

Protein docking studies

A protein model of TbMCA2 was prepared by taking a structure from the Protein Data Bank (PDB [37]; PDB ID 4AF8 [17]) and removing all heteroatoms, including water molecules, and N-terminal residues 31–35 inclusive. Hydrogen atoms were added to this model and a 3D grid was designed with the predicted S_1 binding site [17] at the centre, in order to facilitate receptor docking, using AUTODOCKTOOLS4 [38].

The peptide inhibitor benzoxycarbonyl-Val-Arg-Pro-Arg-fluoromethylketone (Z-VRPR-FMK) has been shown to be an inhibitor of TbMCA2 [17] and was consequently chosen as the ligand for docking studies. The 3D structure of VRPR was taken from the crystal structure of a mammalian paracaspase [20] and AUTODOCKTOOLS4 was used to assign flexible torsions, Gasteiger charges and nonpolar hydrogen atoms. Docking of the ligand into the prepared structure of TbMCA2 was then carried out using AUTODOCK

VINA [39]. All 3D structural alignments were carried out using SSM SUPERPOSE [40] and COOT [41].

Acknowledgements

This work was supported by FAPESP grant 2008/57336-2 to MFMM and by CNPq grant 470044/2010-1 to MFMM. VO was supported by FAPESP grant 2011/51718-3. JCM, KM and CXM were supported by the Wellcome Trust (091790) and the Medical Research Council (0700127). The Wellcome Trust Centre for Molecular Parasitology is supported by core funding from the Wellcome Trust (085349).

References

1 Uren AG, O'Rourke K, Aravind LA, Pisabarro MT, Seshagiri S, Koonin EV & Dixit VM (2000) Identification of paracaspases and metacaspases: two ancient families of caspase-like proteins, one of which plays a key role in MALT lymphoma. *Mol Cell* **6**, 961–967.

2 Rawlings ND, Barrett AJ & Bateman A (2012) MEROPS: the database of proteolytic enzymes, their substrates and inhibitors. *Nucleic Acids Res* **40**, D343–D350.

3 Szallies A, Kubata BK & Duszenko M (2002) A metacaspase of *Trypanosoma brucei* causes loss of respiration competence and clonal death in the yeast *Saccharomyces cerevisiae*. *FEBS Lett* **517**, 144–150.

4 Mottram JC, Helms MJ, Coombs GH & Sajid M (2003) Clan CD cysteine peptidases of parasitic protozoa. *Trends Parasitol* **19**, 182–187.

5 Proto WR, Castanys-Munoz E, Black A, Tetley L, Moss CX, Juliano L, Coombs GH & Mottram JC (2011) *Trypanosoma brucei* metacaspase 4 is a pseudopeptidase and a virulence factor. *J Biol Chem* **286**, 39914–39925.

6 Proto WR, Coombs GH & Mottram JC (2012) Cell death in parasitic protozoa: regulated or incidental? *Nat Rev Microbiol* **11**, 58–66.

7 Helms MJ, Ambit A, Appleton P, Tetley L, Coombs GH & Mottram JC (2006) Bloodstream form *Trypanosoma brucei* depend upon multiple metacaspases associated with RAB11-positive endosomes. *J Cell Sci* **119**, 1105–1117.

8 Vercammen D, Declercq W, Vandenabeele P & Van Breusegem F (2007) Are metacaspases caspases? *J Cell Biol* **179**, 375–380.

9 Moss CX, Westrop GD, Juliano L, Coombs GH & Mottram JC (2007) Metacaspase 2 of *Trypanosoma brucei* is a calcium-dependent cysteine peptidase active without processing. *FEBS Lett* **581**, 5635–5639.

10 Laverriere M, Cazzulo JJ & Alvarez VE (2012) Antagonic activities of *Trypanosoma cruzi* metacaspases affect the balance between cell proliferation, death and differentiation. *Cell Death Differ* **19**, 1358–1369.

11 Gonzalez IJ, Desponds C, Schaff C, Mottram JC & Fasel N (2007) *Leishmania major* metacaspase can replace yeast metacaspase in programmed cell death and has arginine-specific cysteine peptidase activity. *Int J Parasitol* **37**, 161–172.

12 Vercammen D, Van de Cotte B, De Jaeger G, Eeckhout D, Casteels P, Vandepoele K, Vandenberghe I, Van Beeumen J, Inze D & Van Breusegem F (2004) Type II metacaspases Atmc4 and Atmc9 of *Arabidopsis thaliana* cleave substrates after arginine and lysine. *J Biol Chem* **279**, 45329–45336.

13 Watanabe N & Lam E (2005) Two Arabidopsis metacaspases AtMCP1b and AtMCP2b are arginine/lysine-specific cysteine proteases and activate apoptosis-like cell death in yeast. *J Biol Chem* **280**, 14691–14699.

14 Bozhkov PV, Suarez MF, Filonova LH, Daniel G, Zamyatnin AA Jr, Rodriguez-Nieto S, Zhivotovsky B & Smertenko A (2005) Cysteine protease mcII-Pa executes programmed cell death during plant embryogenesis. *Proc Natl Acad Sci USA* **102**, 14463–14468.

15 Pop C & Salvesen GS (2009) Human caspases: activation, specificity, and regulation. *J Biol Chem* **284**, 21777–21781.

16 Watanabe N & Lam E (2011) Calcium-dependent activation and autolysis of Arabidopsis metacaspase 2d. *J Biol Chem* **286**, 10027–10040.

17 McLuskey K, Rudolf J, Proto WR, Isaacs NW, Coombs GH, Moss CX & Mottram JC (2012) Crystal structure of a *Trypanosoma brucei* metacaspase. *Proc Natl Acad Sci USA* **109**, 7469–7474.

18 Wong AH, Yan C & Shi Y (2012) Crystal structure of the yeast metacaspase Yca1. *J Biol Chem* **287**, 29251–29259.

19 Aravind L & Koonin EV (2002) Classification of the caspase-hemoglobinase fold: detection of new families and implications for the origin of the eukaryotic separins. *Proteins* **46**, 355–367.

20 Yu JW, Jeffrey PD, Ha JY, Yang X & Shi Y (2011) Crystal structure of the mucosa-associated lymphoid tissue lymphoma translocation 1 (MALT1) paracaspase region. *Proc Natl Acad Sci USA* **108**, 21004–21009.

21 Garcia-Calvo M, Peterson EP, Rasper DM, Vaillancourt JP, Zamboni R, Nicholson DW & Thornberry NA (1999) Purification and catalytic properties of human caspase family members. *Cell Death Differ* **6**, 362–369.

22 Stennicke HR & Salvesen GS (1997) Biochemical characteristics of caspases-3, -6, -7, and -8. *J Biol Chem* **272**, 25719–25723.

23 Madeo F, Herker E, Maldener C, Wissing S, Lachelt S, Herlan M, Fehr M, Lauber K, Sigrist SJ, Wesselborg S *et al.* (2002) A caspase-related protease regulates apoptosis in yeast. *Mol Cell* **9**, 911–917.
24 Wei Y, Fox T, Chambers SP, Sintchak J, Coll JT, Golec JM, Swenson L, Wilson KP & Charifson PS (2000) The structures of caspases-1, -3, -7 and -8 reveal the basis for substrate and inhibitor selectivity. *Chem Biol* **7**, 423–432.
25 Eichinger A, Beisel HG, Jacob U, Huber R, Medrano FJ, Banbula A, Potempa J, Travis J & Bode W (1999) Crystal structure of gingipain R: an Arg-specific bacterial cysteine proteinase with a caspase-like fold. *EMBO J* **18**, 5453–5462.
26 Shen A, Lupardus PJ, Albrow VE, Guzzetta A, Powers JC, Garcia KC & Bogyo M (2009) Mechanistic and structural insights into the proteolytic activation of *Vibrio cholerae* MARTX toxin. *Nat Chem Biol* **5**, 469–478.
27 Vercammen D, Belenghi B, Van de Cotte B, Beunens T, Gavigan JA, De Rycke R, Brackenier A, Inze D, Harris JL & Van Breusegem F (2006) Serpin1 of *Arabidopsis thaliana* is a suicide inhibitor for metacaspase 9. *J Mol Biol* **364**, 625–636.
28 Suzuki K, Hata S, Kawabata Y & Sorimachi H (2004) Structure, activation, and biology of calpain. *Diabetes* **53**(Suppl 1), S12–S18.
29 Stojdl DF & Clarke MW (1996) *Trypanosoma brucei*: analysis of cytoplasmic Ca^{2+} during differentiation of bloodstream stages *in vitro*. *Exp Parasitol* **83**, 134–146.
30 Goll DE, Thompson VF, Taylor RG & Zalewska T (1992) Is calpain activity regulated by membranes and autolysis or by calcium and calpastatin? *BioEssays* **14**, 549–556.
31 Hirata IC, Sedenho Cezari MH, Nakaie CR, Boshcov P, Ito AS, Juliano MA & Juliano L (1994) Internally quenched fluorogenic protease substrates: solid-phase synthesis and fluorescence spectroscopy of peptides containing ortho-aminobenzoyl/dinitrophenyl groups as donor–acceptor pairs. *Lett Pept Sci* **1994**, 299–308.
32 Araujo MC, Melo RL, Cesari MH, Juliano MA, Juliano L & Carmona AK (2000) Peptidase specificity characterization of C- and N-terminal catalytic sites of angiotensin I-converting enzyme. *Biochemistry* **39**, 8519–8525.
33 Wilkinson GN (1961) Statistical estimations in enzyme kinetics. *Biochem J* **80**, 324–332.
34 Leatherbarrow RJ (2001) Grafit Version 5. Erithacus Software Ltd, Horley, UK.
35 Machado MF, Rioli V, Dalio FM, Castro LM, Juliano MA, Tersariol IL, Ferro ES, Juliano L & Oliveira V (2007) The role of Tyr605 and Ala607 of thimet oligopeptidase and Tyr606 and Gly608 of neurolysin in substrate hydrolysis and inhibitor binding. *Biochem J* **404**, 279–288.
36 Wilkins MR, Gasteiger E, Bairoch A, Sanchez JC, Williams KL, Appel RD & Hochstrasser DF (1999) Protein identification and analysis tools in the ExPASy server. *Methods Mol Biol* **112**, 531–552.
37 Velankar S, Alhroub Y, Best C, Caboche S, Conroy MJ, Dana JM, Fernandez Montecelo MA, Van Ginkel G, Golovin A, Gore SP *et al.* (2012) PDBe: Protein Data Bank in Europe. *Nucleic Acids Res* **40**, D445–D452.
38 Morris GM, Huey R, Lindstrom W, Sanner MF, Belew RK, Goodsell DS & Olson AJ (2009) AutoDock4 and AutoDockTools4: automated docking with selective receptor flexibility. *J Comput Chem* **30**, 2785–2791.
39 Trott O & Olson AJ (2010) AutoDock Vina: improving the speed and accuracy of docking with a new scoring function, efficient optimization, and multithreading. *J Comput Chem* **31**, 455–461.
40 Krissinel E & Henrick K (2004) Secondary-structure matching (SSM), a new tool for fast protein structure alignment in three dimensions. *Acta Crystallogr D Biol Crystallogr* **60**, 2256–2268.
41 Emsley P & Cowtan K (2004) Coot: model-building tools for molecular graphics. *Acta Crystallogr D Biol Crystallogr* **60**, 2126–2132.
42 Baker NA, Sept D, Joseph S, Holst MJ & McCammon JA (2001) Electrostatics of nanosystems: application to microtubules and the ribosome. *Proc Natl Acad Sci USA* **98**, 10037–10041.
43 DeLano WL (2002) The PyMOL Molecular Graphic System. (Schrodinger, LLC, San Carlos, CA), version 1.2r3pre.